

Electrochemical Frequency Modulation: A New Electrochemical Technique for Online Corrosion Monitoring

R.W. Bosch,* J. Hubrecht, W.F. Bogaerts,** and B.C. Syrett***

ABSTRACT

Since a corrosion process is a nonlinear electrochemical phenomenon, a potential perturbation signal by one or more sine waves will generate current responses at more frequencies than the frequencies of the applied signal. Current responses can then be measured, for example, at zero, harmonic, and intermodulation frequencies. This simple principle offers various possibilities for corrosion rate measurements, like the intermodulation or electrochemical frequency modulation (EFM) technique in which the potential perturbation signal consists of two sine waves of different frequencies. With this novel EFM technique, the corrosion rate can be determined from the corrosion system responses at the intermodulation frequencies. With the EFM technique a corrosion rate can be obtained instantaneously, without prior knowledge of the so-called Tafel parameters. The EFM approach requires only a small polarizing signal, and measurements can be completed in a short period. A special advantage of the EFM technique is its capability of inherent data validation control using "causality factors" (parameters introduced for the first time in this paper). It is shown that the EFM technique can be used successfully for corrosion rate measurements under various corrosion conditions, such as mild steel in an acidic environment with and without inhibitors and mild steel in a neutral environment.

KEY WORDS: corrosion rate, electrochemical frequency modulation, impedance, monitoring, nonlinear distortion, polarization resistance, weight loss

INTRODUCTION

Several electrochemical techniques are available to determine corrosion rate, such as the linear polarization resistance (LPR) technique, Tafel-extrapolation, and electrochemical impedance spectroscopy (EIS). For instantaneous corrosion rate measurements, the LPR and EIS techniques can be used if the anodic and cathodic Tafel parameters (b_a and b_c , respectively) are known. The Tafel extrapolation technique permits determination of the corrosion rate and the Tafel parameters, but in most cases it is not suitable for instantaneous corrosion rate measurements because the system must be polarized over a wide potential range, so the measurement is time-consuming and the electrode surface affected by the measurement.

As the corrosion process is nonlinear in nature, a potential perturbation by one or more sine waves will generate responses at more frequencies than the frequencies of the applied signal. Current responses can be measured at zero, harmonic, and intermodulation frequencies. Measuring the direct current (DC) at frequency "zero" is called the Faraday rectification technique. This technique can be used for corrosion rate measurements if at least one of the Tafel parameters is known. The corrosion rate and both Tafel parameters can be obtained with one

Submitted for publication February 2000; in revised form, September 2000.

* SCK•CEN, Nuclear Research Centre Belgium, Boeretang 200, B-2400 Mol, Belgium.

** KU Leuven, Department of Metallurgy and Materials Engineering, De Croylaan 2, B-3001 Heverlee (Leuven), Belgium.

*** Electric Power Research Institute, 3412 Hillview Ave., Palo Alto, CA 94304.

measurement by analyzing the harmonic frequencies.¹⁻² Harmonic analysis has been used for corrosion rate measurements in acid media with and without inhibitors.³⁻⁵ A special application of harmonic analysis is harmonic impedance spectroscopy (HIS), where the harmonic current components are transformed into harmonic impedances. HIS has been used to measure corrosion rates of polarized systems.⁶⁻⁸

In corrosion research, virtually no attention has been given to the intermodulation or electrochemical frequency modulation (EFM) technique. With the EFM technique a potential perturbation by two sine waves of different frequencies is applied to a corroding system. The alternating current (AC) response consists of harmonics at multiples of both frequencies ($\omega_1, 2\omega_1, 3\omega_1, \dots, \omega_2, 2\omega_2, 3\omega_2, \dots$) and of responses at the intermodulation frequencies ($\omega_1 \pm \omega_2, 2\omega_1 \pm \omega_2, 2\omega_1 \pm \omega_1, \dots$). The EFM technique has been used satisfactorily in semiconductor research.⁹⁻¹⁰ Possible application in the electrochemistry field has been mentioned briefly by Rao and Mishra¹¹ and Bertocci.¹² Theoretical work by Mészáros and Dévay,¹³ using a modified Bessel function, resulted in modeling of the intermodulation response for an activation-controlled corrosion process. A previously published paper revealed that mathematical modeling with a simple Taylor expansion leads to similar results.¹⁴ That paper also showed that corrosion rates could be properly measured in an acidic environment.

The research presented in this paper will go one step further with the EFM technique, introducing the causality factors. With the causality factors the quality of the experimental EFM data can be verified. The EFM technique will be used here for online monitoring of the corrosion rate of various types of corroding systems. The EFM corrosion rates are shown to be in agreement with more established techniques for corrosion rate measurements like Tafel extrapolation, LPR, and weight loss measurements. The causality factor is also shown to be a useful measure for validating the data quality.

THEORY

Principle of the EFM Technique

With the EFM technique, a potential perturbation by two sine waves of different frequencies is applied to a corroding system. The AC-current response resulting from this perturbation consists of current components of different frequencies. Since a corrosion process is nonlinear in nature, responses are generated at more frequencies than the frequencies of the applied signal. Current responses can be measured at zero, harmonic, and intermodulation frequencies. The principle of the EFM technique is illustrated in Figure 1.

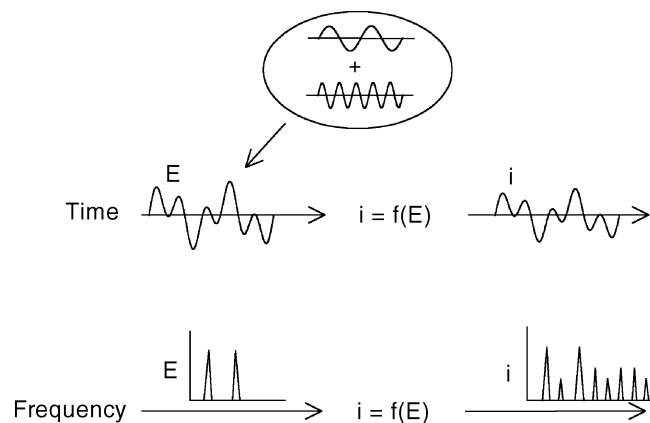


FIGURE 1. Principle of the EFM technique.

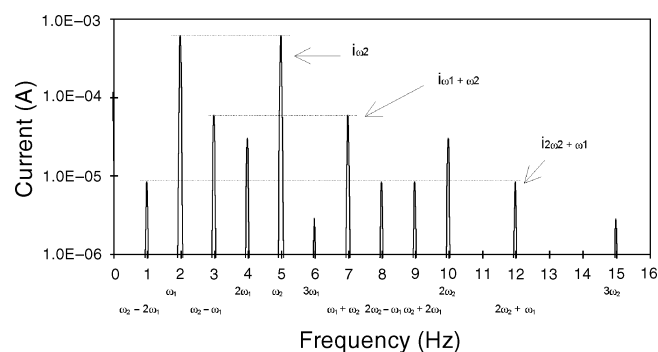


FIGURE 2. Harmonic and intermodulation frequencies resulting from the basic frequencies 2 Hz and 5 Hz.

A schematic of a frequency spectrum of an EFM current response, illustrating the different harmonic and intermodulation frequencies, is depicted in Figure 2.

Figures 3 and 4 show some results obtained from a real corroding system (i.e., mild steel in sulfuric acid [H_2SO_4] solution) using a perturbation signal with an amplitude of 20 mV for both frequencies and perturbation frequencies of 0.2 Hz and 0.5 Hz. The choice for the frequencies of 0.2 Hz and 0.5 Hz was based on three arguments. First, the harmonics and intermodulation frequencies should not influence each other. Second, the frequency should be as low as possible to avoid influence of the capacitive behavior of the electrochemical double layer. Third, the frequency should be as large as possible to reduce the time needed to perform a measurement. While these arguments do not allow the selection of "perfect" frequencies, the chosen frequencies were considered a reasonable compromise.

Figure 3 shows the frequency spectrum of the potential signal measured on the corrosion cell. Figure 4 shows the corresponding current response in the frequency spectrum. The harmonic and intermodulation peaks are clearly visible and are much larger than the background noise. Analysis of

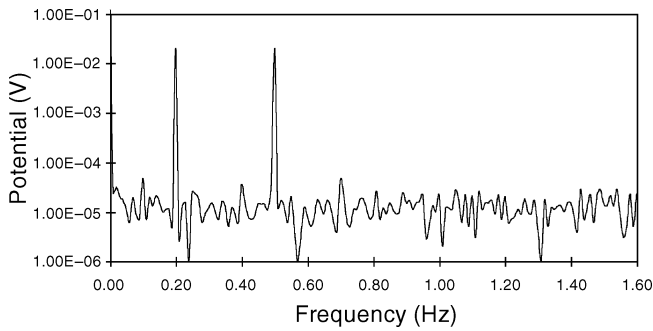


FIGURE 3. Frequency spectrum of the potential signal measured for mild steel in 0.05 M H_2SO_4 at the corrosion potential.

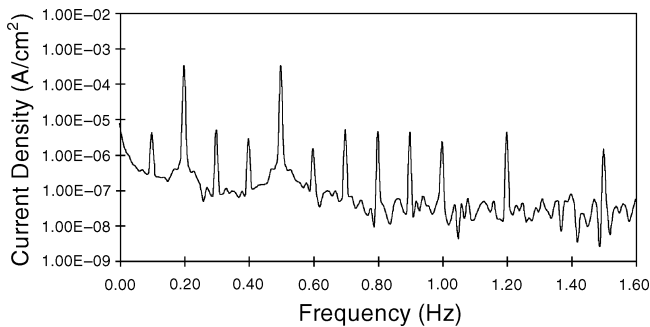


FIGURE 4. Frequency spectrum of the current response of mild steel in 0.05 M H_2SO_4 .

the peaks at the intermodulation frequencies can reveal the corrosion rate and Tafel parameters.

MODELING OF THE EFM RESPONSE WITH A TAYLOR EXPANSION

Activation-Controlled Corrosion Systems

The mathematical treatment for the EFM technique previously published¹⁴⁻¹⁵ should be repeated, as these results are necessary to define the causality factors. The causality factors are introduced because they can be used to verify the quality of the experimental EFM data. A potential perturbation consisting of two sine waves of different frequencies is applied to a corroding system:

$$\eta = U_o \sin \omega_1 t + U_o \sin \omega_2 t \quad (1)$$

where η is the overpotential, U_o the amplitude of the potential perturbation, and ω_1 and ω_2 the (angular) perturbation frequencies in rad/s. Note that $\omega = 2\pi f$ with the frequency f in Hertz. Since a corroding process is nonlinear in nature, the current response resulting from this potential perturbation contains nonlinear components. The frequency spectrum of the current response thus contains higher harmonics ($2\omega_1, 3\omega_1, \dots, 2\omega_2, 3\omega_2, \dots$) and intermodulation components. The latter are the responses measured at an-

gular frequencies $\omega_1 \pm \omega_2, 2\omega_1 \pm \omega_2, \omega_1 \pm 2\omega_2$, etc. Analysis of these components at different frequencies can result in the corrosion rate and Tafel parameters. The derivation of the higher-order response to the potential perturbation starts with the current-potential equation of a corroding process following Tafel behavior:

$$i = i_{\text{corr}} \left[\exp\left(\frac{\eta}{\beta_a}\right) - \exp\left(-\frac{\eta}{\beta_c}\right) \right] \quad (2)$$

where i_{corr} is the corrosion current density, β_a the anodic Tafel parameter, and β_c the cathodic Tafel parameter. Note that $\beta_a = \frac{b_a}{\ln 10}$ and $\beta_c = \frac{b_c}{\ln 10}$. Throughout the text, β_a and β_c will be used when mathematical modeling is carried out to avoid using the factor $\ln 10$ repeatedly. For numerical simulation, the b_a and b_c values are used because they are more common (compare $b_c = 120$ mV/decade with $\beta_c = 52.1$ mV). The potential perturbation described with Equation (1) is substituted in Equation (2), resulting in Equation (3):

$$i = i_{\text{corr}} \left[\exp\left(\frac{U_o \sin \omega_1 t}{\beta_a}\right) \exp\left(\frac{U_o \sin \omega_2 t}{\beta_a}\right) - \exp\left(-\frac{U_o \sin \omega_1 t}{\beta_c}\right) \exp\left(-\frac{U_o \sin \omega_2 t}{\beta_c}\right) \right] \quad (3)$$

The exponential parts are expanded in a Taylor series:

$$\exp\left(\frac{U_o \sin \omega_1 t}{\beta_a}\right) = 1 + \frac{U_o \sin \omega_1 t}{\beta_a} + \frac{1}{2} \left(\frac{U_o \sin \omega_1 t}{\beta_a}\right)^2 + \frac{1}{6} \left(\frac{U_o \sin \omega_1 t}{\beta_a}\right)^3 + \dots \quad (4)$$

and:

$$\exp\left(-\frac{U_o \sin \omega_1 t}{\beta_c}\right) = 1 - \frac{U_o \sin \omega_1 t}{\beta_c} + \frac{1}{2} \left(\frac{U_o \sin \omega_1 t}{\beta_c}\right)^2 - \frac{1}{6} \left(\frac{U_o \sin \omega_1 t}{\beta_c}\right)^3 + \dots \quad (5)$$

For the exponential parts $\exp\left(\frac{U_o \sin \omega_2 t}{\beta_a}\right)$ and $\exp\left(-\frac{U_o \sin \omega_2 t}{\beta_c}\right)$ an analogous treatment is valid. Using trigonometric relationships (exemplified in Equations [6] and [7]), Equation (3) is written as a series of sines and cosines with different frequencies:

$$\left(\frac{U_o \sin \omega_1 t}{\beta_a}\right)^2 = \frac{1}{2} \left(\frac{U_o}{\beta_a}\right)^2 - \frac{1}{2} \left(\frac{U_o}{\beta_a}\right)^2 \cos 2\omega_1 t \quad (6)$$

and:

$$\left(\frac{U_o \sin \omega_1 t}{\beta_a}\right)^3 = \frac{3}{4}\left(\frac{U_o}{\beta_a}\right)^3 \sin \omega_1 t - \frac{1}{4}\left(\frac{U_o}{\beta_a}\right)^3 \sin 3\omega_1 t \quad (7)$$

These relationships are also used for the terms with ω_2 and β_c . Using the Taylor-series expansion for $\exp(x)$ to the third order and some algebraic manipulations yields an equation of the following form:

$$\begin{aligned} i = & i_{fr} + i_{\omega_1} \sin \omega_1 t + i_{\omega_2} \sin \omega_2 t - i_{2\omega_1} \cos 2\omega_1 t - \\ & i_{2\omega_2} \cos 2\omega_2 t - i_{3\omega_1} \sin 3\omega_1 t - i_{3\omega_2} \sin 3\omega_2 t + \\ & i_{\omega_2 \pm \omega_1} \cos(\omega_2 t - \omega_1 t) - i_{\omega_2 \pm \omega_1} \cos(\omega_2 t + \omega_1 t) + \\ & i_{2\omega_2 \pm \omega_1} \sin(2\omega_2 t - \omega_1 t) - i_{2\omega_2 \pm \omega_1} \sin(2\omega_2 t + \omega_1 t) + \\ & i_{2\omega_1 \pm \omega_2} \sin(2\omega_1 t - \omega_2 t) - i_{2\omega_1 \pm \omega_2} \sin(2\omega_1 t + \omega_2 t) \end{aligned} \quad (8)$$

where i_{fr} is the Faraday rectification current, $i_{2\omega_1}$ and $i_{2\omega_2}$ are the harmonic currents at angular frequencies $2\omega_1$ and $2\omega_2$, and i_{ω_1} and i_{ω_2} are the intermodulation currents at angular frequencies ω_1 and ω_2 , respectively. $i_{\omega_2 + \omega_1}$ and $i_{\omega_2 - \omega_1}$ are the intermodulation currents at angular frequencies $\omega_2 + \omega_1$ and $\omega_2 - \omega_1$, etc. The harmonic and intermodulation parts in this equation are equal to the following:

$$i_{\omega_1} = i_{\omega_2} = i_{corr} \left[\frac{U_o}{\beta_a} + \frac{U_o}{\beta_c} \right] \quad (9)$$

$$i_{2\omega_1} = i_{2\omega_2} = \frac{1}{4} i_{corr} \left[\left(\frac{U_o}{\beta_a} \right)^2 - \left(\frac{U_o}{\beta_c} \right)^2 \right] \quad (10)$$

$$i_{3\omega_1} = i_{3\omega_2} = \frac{1}{24} i_{corr} \left[\left(\frac{U_o}{\beta_a} \right)^3 + \left(\frac{U_o}{\beta_c} \right)^3 \right] \quad (11)$$

$$i_{\omega_2 \pm \omega_1} = \frac{1}{2} i_{corr} \left[\left(\frac{U_o}{\beta_a} \right)^2 - \left(\frac{U_o}{\beta_c} \right)^2 \right] \quad (12)$$

$$i_{2\omega_2 \pm \omega_1} = i_{2\omega_1 \pm \omega_2} = \frac{1}{8} i_{corr} \left[\left(\frac{U_o}{\beta_a} \right)^3 + \left(\frac{U_o}{\beta_c} \right)^3 \right] \quad (13)$$

Solving Equations (9), (12), and (13) for i_{corr} , β_a , and β_c , the following expressions are obtained, assuming that ω_2 is $> \omega_1$ (and $\beta_a < \beta_c$):

$$i_{corr} = \frac{i_{\omega_1, \omega_2}^2}{2\sqrt{8i_{\omega_1, \omega_2} i_{2\omega_2 \pm \omega_1} - 3i_{\omega_2 \pm \omega_1}^2}} \quad (14)$$

TABLE 1

Data Obtained with the EFM Technique for Mild Steel in 0.05 M H₂SO₄

Current Component	Angular Frequency (rad/s)	Frequency (Hz)	Current Density (A/cm ²)
i_{ω_1, ω_2}	ω_1	0.2	3.19×10^{-4}
	ω_2	0.5	3.19×10^{-4}
$i_{\omega_2 \pm \omega_1}$	$\omega_2 - \omega_1$	0.3	4.89×10^{-6}
	$\omega_2 + \omega_1$	0.7	4.98×10^{-6}
$i_{2\omega_2 \pm \omega_1}$	$\omega_2 - 2\omega_1$	0.1	4.10×10^{-6}
	$2\omega_2 - \omega_1$	0.8	4.30×10^{-6}
	$\omega_2 + 2\omega_1$	0.9	4.21×10^{-6}
	$2\omega_2 + \omega_1$	1.2	4.17×10^{-6}
$i_{2\omega_1}$	$2\omega_1$	0.4	2.76×10^{-6}
$i_{2\omega_2}$	$2\omega_2$	1.0	2.24×10^{-6}
$i_{3\omega_1}$	$3\omega_1$	0.6	1.44×10^{-6}
$i_{3\omega_2}$	$3\omega_2$	1.5	1.35×10^{-6}

$$\beta_a = \frac{i_{\omega_1, \omega_2} U_o}{i_{\omega_2 \pm \omega_1} + \sqrt{8i_{\omega_1, \omega_2} i_{2\omega_2 \pm \omega_1} - 3i_{\omega_2 \pm \omega_1}^2}} \quad (15)$$

$$\beta_c = \frac{i_{\omega_1, \omega_2} U_o}{-i_{\omega_2 \pm \omega_1} + \sqrt{8i_{\omega_1, \omega_2} i_{2\omega_2 \pm \omega_1} - 3i_{\omega_2 \pm \omega_1}^2}} \quad (16)$$

The current components mentioned in Equations (14) through (16) are measured at multiple frequencies in the frequency spectrum of the current response. The component at the perturbation frequencies i_{ω_1, ω_2} is measured at angular frequency ω_1 or ω_2 . The intermodulation component $i_{\omega_2 \pm \omega_1}$ is measured at angular frequency $\omega_2 - \omega_1$ or $\omega_2 + \omega_1$. The intermodulation component $i_{2\omega_2 \pm \omega_1}$ is measured at angular frequency $2\omega_2 + \omega_1$, $2\omega_2 - \omega_1$, $\omega_2 + 2\omega_1$, or $\omega_2 - 2\omega_1$, which is summarized in Figure 2 and Table 1.

For the calculation of the corrosion rate and Tafel parameters in this investigation, the current components measured at corresponding frequencies are averaged and then used in Equations (14) through (16).

Diffusion-Controlled Corrosion Systems

For a corrosion process with the cathodic reaction completely controlled by diffusion, the cathodic Tafel parameter is infinite ($\beta_c \rightarrow \infty$). The current-potential relation corresponding to this situation is thus:

$$i = i_{corr} \left[\exp\left(\frac{\eta}{\beta_a}\right) - 1 \right] \quad (17)$$

The potential signal of Equation (1) is substituted in Equation (17), and, after treatment as before, the following equations for i_{corr} and β_a are obtained:

$$i_{\text{corr}} = \frac{i_{\omega_1, \omega_2}^2}{2i_{\omega_2 \pm \omega_1}} \quad (18)$$

$$\beta_a = \frac{i_{\omega_1, \omega_2}}{2i_{\omega_2 \pm \omega_1}} U_o \quad (19)$$

These equations can be used to calculate a corrosion rate when the cathodic reaction is diffusion-controlled.

Passivating Systems

For a corrosion process with complete passivation of the anodic reaction, the anodic Tafel parameter is infinite ($\beta_a \rightarrow \infty$). The current-potential relation corresponding with this situation is thus:

$$i = i_{\text{corr}} \left[1 - \exp\left(-\frac{\eta}{\beta_c}\right) \right] \quad (20)$$

The potential signal of Equation (1) is substituted in Equation (20), and, after treatment as before, the following equations for i_{corr} and β_c are obtained:

$$i_{\text{corr}} = \frac{i_{\omega_1, \omega_2}^2}{2i_{\omega_2 \pm \omega_1}} \quad (21)$$

$$\beta_c = \frac{i_{\omega_1, \omega_2}}{2i_{\omega_2 \pm \omega_1}} U_o \quad (22)$$

These equations can be used to calculate a corrosion rate when the anodic reaction is completely passivated.

Quality Control with the Causality Factor

The frequency spectrum of the current response contains components at harmonic and intermodulation frequencies. The harmonic components $i_{2\omega_1}$ and $i_{2\omega_2}$ are measured at angular frequencies $2\omega_1$ and $2\omega_2$. The harmonic components $i_{3\omega_1}$ and $i_{3\omega_2}$ are measured at angular frequencies $3\omega_1$ and $3\omega_2$. The intermodulation components $i_{\omega_2 + \omega_1}$ are measured at angular frequencies $\omega_2 \pm \omega_1$, and the intermodulation components $i_{2\omega_2 \pm \omega_1}$ and $i_{2\omega_1 \pm \omega_2}$ are measured at angular frequencies $2\omega_2 \pm \omega_1$ and $2\omega_1 \pm \omega_2$, respectively. Between these components a relationship exists. It can be shown that the harmonic and intermodulation components have the following relationship (Equations [10] through [13]):

$$i_{\omega_2 \pm \omega_1} = 2i_{2\omega_1} = 2i_{2\omega_2} \quad (23)$$

and:

$$i_{2\omega_2 \pm \omega_1} = i_{2\omega_1 \pm \omega_2} = 3i_{3\omega_1} = 3i_{3\omega_2} \quad (24)$$

The causality factors, which are based on these relationships, are defined as follows:

$$\text{Causality factor (2): } \frac{i_{\omega_2 \pm \omega_1}}{i_{2\omega_1}} \quad (25)$$

$$\text{Causality factor (3): } \frac{i_{2\omega_2 \pm \omega_1}}{i_{3\omega_1}} \quad (26)$$

The current components in Equations (25) and (26) are interchangeable with the current components in Equations (23) and (24), respectively. Causality factor (2) = 2 and Causality factor (3) = 3 if there is a relation between the perturbation signal and the distorted response signal. The idea behind this causality factor is that it can be used to check the validity of the data. The causality factor is calculated from the frequency spectrum of the current response. If the causality factors differ significantly from the theoretical values of 2 and 3, it can be deduced that the measurements are influenced by noise. If the causality factors are approximately equal to the predicted values of 2 and 3, there is a causal relationship between the perturbation signal and the response signal. Then the data are assumed to be reliable.

An example of a corroding system is the corrosion of mild steel in H_2SO_4 solution. Figure 4 shows the frequency spectrum of the current response of this corroding system resulting from a potential signal of 20 mV and frequencies of 0.2 Hz and 0.5 Hz. Analysis of this frequency spectrum produced the results in Table 1 where all the current components and corresponding frequencies are shown.

These data are used to calculate the corrosion current density, the Tafel parameters, and the causality factors with Equations (14), (15), (16), (25), and (26). Harmonic and intermodulation current components measured at multiple frequencies are averaged (i.e., $i_{3\omega_1}$ and $i_{2\omega_2 \pm \omega_1}$), following from:

$$i_{3\omega_1} = \frac{1.44 \times 10^{-6} + 1.35 \times 10^{-6}}{2} = 1.39 \times 10^{-6} \text{ A / cm}^2 \quad (27)$$

$$i_{2\omega_2 \pm \omega_1} = \frac{4.1 \times 10^{-6} + 4.3 \times 10^{-6} + 4.21 \times 10^{-6} + 4.17 \times 10^{-6}}{4} = 4.20 \times 10^{-6} \text{ A / cm}^2$$

Causality factor (3) is then calculated as follows:

$$\text{Causality factor (3): } \frac{i_{2\omega_2 \pm \omega_1}}{i_{3\omega_1}} = \frac{4.20 \times 10^{-6}}{1.39 \times 10^{-6}} = 3.01 \quad (28)$$

All results are shown in Table 2.

The causality factors indicate that the measured data are of good quality. The corrosion rate is in agreement with other techniques.

Influence of Perturbation Amplitude and Frequency on EFM Corrosion Rate and Causality Factors

The equations derived in the previous paragraphs are based on a partially expanded Taylor series. Terms of the Taylor series with an order > 3 are neglected. Therefore, the equations are valid only when the amplitude of the potential signal is sufficiently small (i.e., the amplitude should not exceed the low-distortion region). More precisely, the ratio between the perturbation amplitude and the Tafel parameter should be much less than 1:

$$\frac{U_o}{\beta_a} \ll 1, \quad \frac{U_o}{\beta_c} \ll 1 \quad (29)$$

A mathematical calculation of the introduced error, depending on the amplitude size, was given in a previous publication.¹⁴ Here, an experimental investigation of this sensitivity was carried out for the corroding system of mild steel in H_2SO_4 solution. This system is assumed to be activation-controlled, so Equation (14) is valid for calculating the corrosion rate. Different amplitudes and frequencies were used to obtain the EFM data. Table 3 shows the results.

With increasing amplitude the corrosion rate determined with the EFM technique appeared to increase. The frequency hardly influenced the results. A small amplitude was also preferred to avoid significant attack of the working electrode. For the EFM measurements, an amplitude just large enough to generate three harmonics in the current response was chosen.

Equation (3), representing an activation-controlled corrosion system, was also applied to generate some artificial EFM data using a Fourier transform of the current response. Some random noise was added to the current response, representing the background noise always present in field conditions. As-

[†] Trade name.

TABLE 2

Corrosion Rate, Tafel Parameters, and Causality Factors for Mild Steel in 0.05 M H_2SO_4 , Determined with the EFM Technique

Parameter	Value
Corrosion current density (A/cm^2)	4.93×10^{-4}
Anodic Tafel parameter (mV/decade)	135
Cathodic Tafel parameter (mV/decade)	149
Causality factor (2)	1.97
Causality factor (3)	3.01

suming a corroding system with $i_{corr} = 1.10^{-4} A/cm^2$, $b_a = 60$ mV/decade, and $b_c = 120$ mV/decade, the causality factors are calculated according to Equations (25) and (26). Figure 5 shows the causality factors versus the amplitude.

For small values of the potential perturbation amplitude, the causality factors were clearly distorted by background noise. For larger values there was a plateau region where the causality factors were independent of the amplitude. For very large values of the potential perturbation amplitude (> 50 mV) the causality factors differed significantly from their plateau values of 2 and 3. This latter deviation was attributed to the fact that the ratio between the perturbation amplitude and the Tafel parameter was no longer much smaller than 1 (as stated previously, Equation [27]). This plateau region was important because the EFM equations were only valid in this region.

EXPERIMENTAL PROCEDURES

The configuration shown in Figure 6 was used to perform the EFM technique.

The experimental setup included a computer with a computer-controlled potentiostat. All the software programs necessary to perform the measurements were developed in-house with the graphical programming language LabView[†].¹⁶ A typical experiment was performed as follows.

The corrosion potential was measured and the potentiostat was set to this value. A potential perturbation was generated by the computer and fed to the

TABLE 3

Corrosion Rates Determined with the EFM-Technique for Mild Steel in 0.05 M H_2SO_4 Solution with Different Amplitudes and Frequencies

Amplitude (mV)	Corrosion Current Density (mA/cm^2)		
	2 Hz and 5 Hz	0.2 Hz and 0.5 Hz	0.02 Hz and 0.05 Hz
10	0.47	0.47	0.4
20	0.49	0.48	0.43
50	0.77	0.76	0.69
100	1.82	1.76	1.81

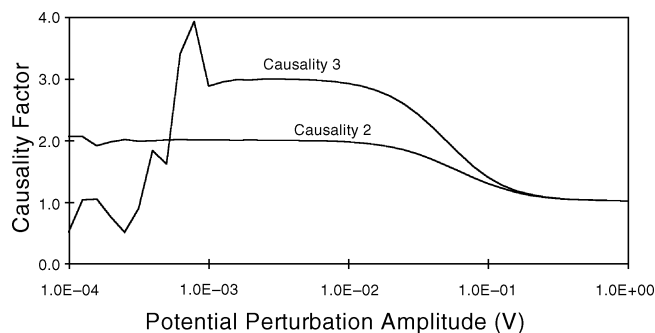


FIGURE 5. Influence of the potential perturbation amplitude on the causality factors calculated for $i_{\text{corr}} = 1.10^{-4} \text{ A/cm}^2$, $b_a = 60 \text{ mV/decade}$, and $b_c = 120 \text{ mV/decade}$.

potentiostat. The current response was measured by the potentiostat and then analyzed by the computer. With a Fourier transform the current response was transformed to the frequency domain. A sub-VI (amplitude and phase spectrum) computed the single-sided amplitude spectrum magnitude.¹⁷⁻¹⁹ Currents were presented as current densities since this allows direct calculation of the corrosion rate with Equation (14). The current densities of interest were selected and saved to the hard disk. The corrosion rate was calculated afterward.

The layout of the computer interface for the EFM measurements is shown in Figure 7. Here, "Ecorr" shows the measured corrosion potential and its average value over 10 s ("Ecorr Average"). "Vmeas" shows the potential perturbation measured at the corrosion cell. "Imeas" shows the current response measured at the corrosion cell. "FFT Imeas" shows the frequency spectrum of the current response. The "Intermodulation and Harmonic Table" shows the frequencies of interest and corresponding current components. "Results" shows the calculated corrosion rate (i_{corr}), Tafel parameters (b_a and b_c), and causality factors (Causality 2 and Causality 3). The upper three blocks on the left side show test parameters related to the measurement itself. The sampling

frequency ($f_s = 1/\text{dt}$) and total number of data points (N) can be adjusted. For the measurements with 0.2 Hz and 0.5 Hz, $N = 1,000$ and $\text{dt} = 0.1 \text{ s}$ were used (i.e., the sampling frequency was 10 Hz). This resulted in a frequency interval of $\Delta f = 1/N\text{dt} = 0.01 \text{ Hz}$. The amplitude-frequency spectrum contained all current components at $m \cdot 0.01$ ($m = \text{integer}$) frequencies, which includes all harmonic and intermodulation components of interest.

RESULTS AND DISCUSSION

Mild Steel in H_2SO_4

Experiments were performed on mild steel in 0.05 M H_2SO_4 in a standard three-electrode configuration. Every hour the corrosion rate was measured with the EFM technique. Figure 8 shows the corrosion rates and causality factors obtained over 60 h.

The corrosion current slightly increased with time. This behavior was expected as the active surface area of the electrode increased with progressing corrosion. The causality factors had values of ≈ 2 and 3, so the calculated corrosion rates were based on reliable data. Causality factor (3) showed some spikes for times higher than 30 h, which was attributed to background noise. Causality factor (3) was most sensitive because this contained the third harmonic. These results were then compared with results from LPR measurements, weight loss measurements, and solution analysis (atomic absorption spectroscopy [AAS]).

The corrosion rates obtained with LPR measurements were calculated with Tafel parameters obtained both from polarization curves produced in separate experiments and from the EFM results (calculated with Equations [15] and [16]). The Tafel parameters obtained from polarization curves were 40 mV/decade for the anodic Tafel parameter and 120 mV/decade for the cathodic Tafel parameter. Figure 9 compares the corrosion rates obtained by the different techniques.

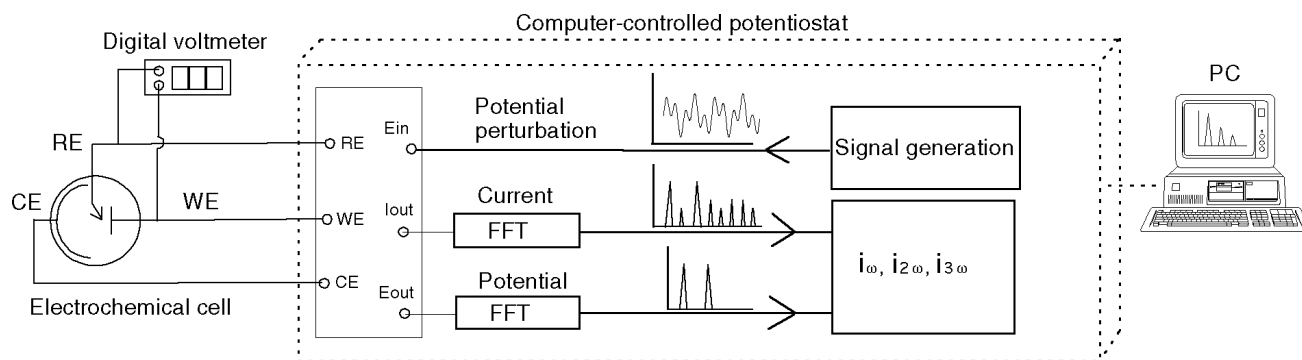


FIGURE 6. Experimental setup.



FIGURE 7. Layout of the computer interface for the harmonic and intermodulation measurements with a programmable potentiostat.

The error bars for the EFM and LPR techniques were based on the range of corrosion rates measured during one experiment, while the error bars for the weight loss and solution analysis were based on multiple experiments, which helps explain the differences. Corrosion rates obtained by the various techniques agree.

Corrosion Inhibition with an Organic Inhibitor

Experiments were performed with mild steel in deaerated 0.5 M H_2SO_4 with various concentrations of hexamethylene tetramine ($C_6H_{12}N_4$), which was added to inhibit the corrosion process.²⁰⁻²¹ Three different test solutions were used: 0.5 M H_2SO_4 without inhibitor, 0.5 M H_2SO_4 with 0.2 mmol inhibitor, and 0.5 M H_2SO_4 with 2 mmol inhibitor. Figures 10 and 11 show the results of the EIS tests.

The influence of the inhibitor was clearly demonstrated by the differences in diameter of the semi-circles, as shown in Figure 10. With increasing inhibitor concentration, the diameter increased, which means that the polarization resistance also increased. The Bode diagram shows that, for fre-

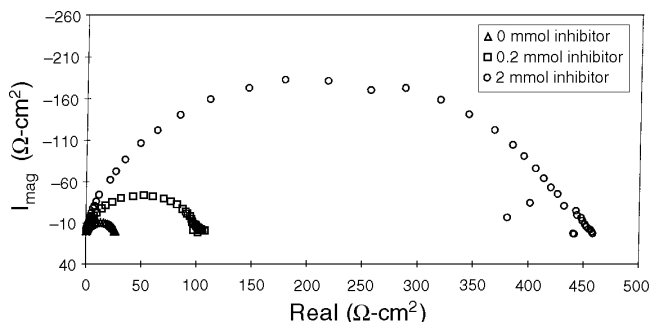


FIGURE 10. Nyquist diagrams obtained for mild steel in deaerated 0.5 M H_2SO_4 and different concentrations of inhibitor.

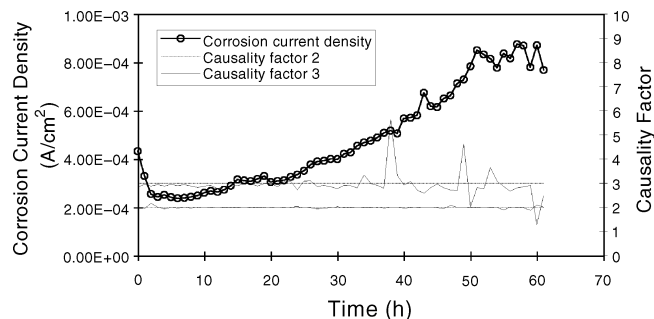


FIGURE 8. Corrosion current density and causality factors determined with EFM of mild steel in 0.05 M H_2SO_4 .

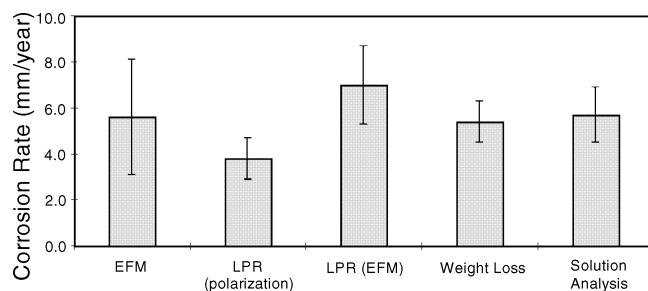


FIGURE 9. Comparison of corrosion rates of mild steel in 0.05 M H_2SO_4 using different techniques.

quencies < 1 Hz, the modulus of the impedance hardly changed with the perturbation frequency. The polarization resistance was obtained from the EIS data using the following relationship:⁷

$$R_p = |Z(j\omega)|_{\omega \rightarrow 0} - |Z(j\omega)|_{\omega \rightarrow \infty} \quad (30)$$

where R_p is the polarization resistance, $|Z(j\omega)|_{\omega \rightarrow 0}$ the low frequency limit of the impedance, and $|Z(j\omega)|_{\omega \rightarrow \infty}$ the high frequency limit of the impedance. To calculate the corrosion rate with the polarization resistance, the Tafel parameters have to be known. Polarization curves were recorded and the Tafel regions were extrapolated to the corrosion potential to

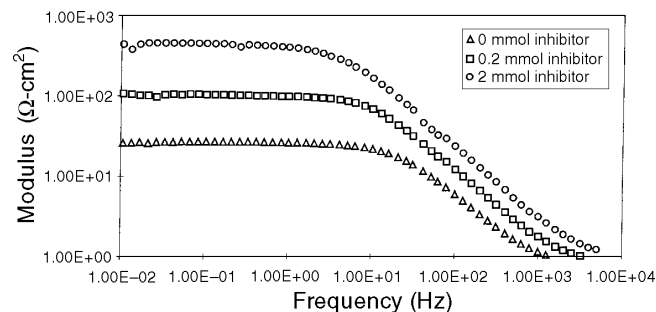


FIGURE 11. Bode diagrams obtained for mild steel in deaerated 0.5 M H_2SO_4 and different concentrations of inhibitor.

TABLE 4
Corrosion Rates and Tafel Parameters Obtained with EIS and Tafel Extrapolation for Mild Steel in 0.5 M H₂SO₄ with Different Concentrations of Inhibitor

Solution composition	EIS	Tafel Extrapolation (Polarization Curves)		
	Corrosion current density (mA/cm ²)	Corrosion current density (mA/cm ²)	Anodic Tafel parameter (mV/decade)	Cathodic Tafel parameter (mV/decade)
0.5 M H ₂ SO ₄	0.45 ± 0.06	0.43 ± 0.12	37 ± 7	107 ± 8
0.5 M H ₂ SO ₄ + 0.2 mmol inhibitor	0.13 ± 0.03	0.11 ± 0.02	35 ± 2	113 ± 2
0.5 M H ₂ SO ₄ + 2 mmol inhibitor	0.034 ± 0.031	0.018 ± 0.016	54 ± 1	109 ± 11

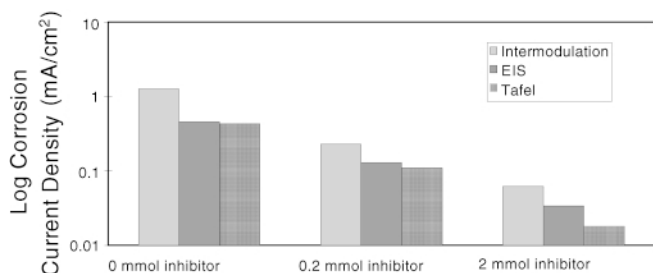


FIGURE 12. Comparison of corrosion rates obtained with EFM, EIS, and polarization curves (Tafel extrapolation).

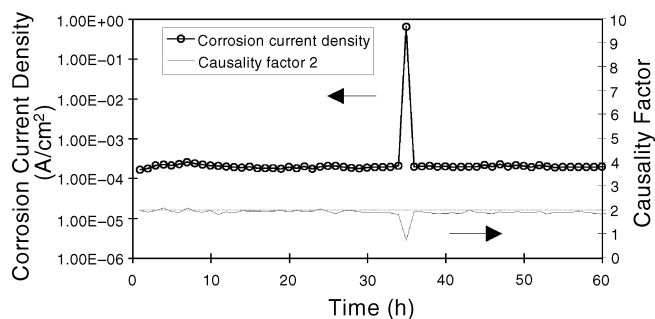


FIGURE 13. Corrosion current density and causality factors determined with EFM of mild steel in 1 M NaCl.

obtain the Tafel parameters and another value of the corrosion rate. The corrosion rates and Tafel parameters determined from EIS and Tafel extrapolation are shown in Table 4. To calculate the corrosion rate from the polarization resistance obtained with EIS, the Tafel parameters obtained from the polarization curves were used.

Table 4 shows that all the corrosion rates decreased with increasing inhibitor concentration. The values of the Tafel parameters were hardly influenced by the inhibitor. For the corrosion of iron in H₂SO₄, an anodic Tafel parameter of 40 mV/decade and a cathodic Tafel parameter of 120 mV/decade were generally reported. The results obtained from the polarization measurements were in reasonable agreement with these values. In Figure 12, the corrosion rates, obtained with the three different techniques

versus the inhibitor concentration, are shown in a histogram.

The three different techniques showed similar behavior. With increasing inhibitor concentration the corrosion rate decreased. Based on these results, the EFM technique appears capable of monitoring the corrosion inhibition of mild steel in H₂SO₄ solution with different concentrations of inhibitor.

Mild Steel in Sodium Chloride Solution

Experiments were performed on mild steel in 1 M sodium chloride (NaCl) open to the air. It was assumed that the cathodic reaction was mainly the reduction of oxygen from the electrolyte solution and that this reaction was more or less controlled by diffusion. Figure 13 shows results of the EFM measurements obtained during a 60-h period.

The corrosion rate was calculated with Equation (18), assuming complete diffusion control. The corrosion rate was more or less constant during the 60 h of the experiment. Causality factor (2) showed correct values for most of the test period. There was one erroneous measurement, which was clearly indicated by a reduction of the causality factor to < 1. Note that Causality factor (3) is no longer plotted because the intermodulation current was not needed to calculate the corrosion rate using Equation (18). LPR measurements were carried out assuming that the cathodic reaction was under diffusion control ($\beta_c \rightarrow \infty$) and that the anodic parameter was 120 mV/decade. Weight loss measurements and AAS were also carried out. Figure 14 shows the average corrosion rates obtained using the different techniques. The EFM experiments were performed using potential perturbation frequencies of 0.02 Hz and 0.05 Hz, to make sure (or at least promote) that the corrosion rate was diffusion-controlled.

For these data there is agreement among the corrosion rates obtained by various techniques. However, the practical application of such low-frequency measurements may be difficult because of the long measurement time.

To investigate the sensitivity of the EFM technique to changes in the corrosiveness of the environment, experiments were performed with different

oxygen concentrations and hydrodynamic conditions. Experiments were performed on mild steel in 0.5 M NaCl. Oxygen was removed by purging pure nitrogen gas through the electrolyte solution. To increase the oxygen concentration, pure oxygen was purged through the electrolyte solution. During an experiment, the oxygen concentration was varied, while the corrosion rate was measured every minute. Figure 15 shows results of such an experiment.

The EFM technique clearly followed the changes in oxygen concentration. The corrosion rates were calculated with Equation (18) (diffusion model). The causality factor confirmed that the data quality was good except between 100 min and 150 min when a temporary disturbance can be noticed, indicating that the data are not reliable. Figure 16 shows results indicating that the hydrodynamic conditions were changed during the experiment.

The corrosion rate followed the changes in hydrodynamic conditions. The causality factor shows that the data after 450 min are not reliable. Subsequent inspection showed that the salt bridge was poorly connected to the reference electrode.

CONCLUSIONS

❖ With the EFM technique, the “instantaneous” corrosion rate can be obtained fairly quickly without prior knowledge of the Tafel parameters, and with only a small polarizing signal. The causality factor, introduced in this work, is a parameter which is suitable for validation of the experimental data. Experimental results show that there is a clear correlation between the causality factor and the quality of the experimental data. To obtain reliable corrosion rates, however, selection of the proper corrosion model to treat the experimental data is required. Experimental results obtained for mild steel in H_2SO_4 solution with and without inhibitor are in agreement with more established techniques for corrosion rate measurement, such as LPR, EIS, and weight loss measurements.

❖ Corrosion rates obtained for mild steel in different solutions with EFM, LPR, and weight loss measurements are in reasonable agreement.

❖ The EFM technique is capable of monitoring differences in the corrosiveness of the environment, like changes in the oxygen concentration and hydrodynamic conditions. The advantages of the EFM technique (direct, nondestructive, quick measurement of corrosion rate and data validation) make it an ideal candidate for online corrosion-monitoring applications.

ACKNOWLEDGMENTS

The authors acknowledge the Electric Power Research Institute for financial support of this work.

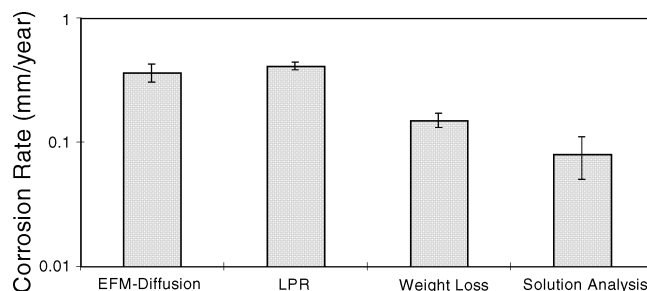


FIGURE 14. Comparison of corrosion rates of mild steel in 1 M NaCl (EFM frequencies 0.02 Hz and 0.05 Hz).

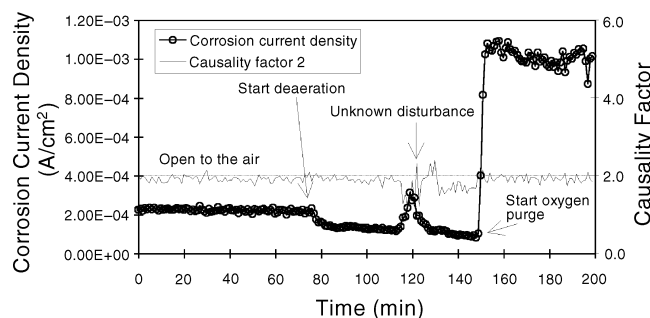


FIGURE 15. Corrosion rates for mild steel in 0.5 M NaCl under different aeration conditions.

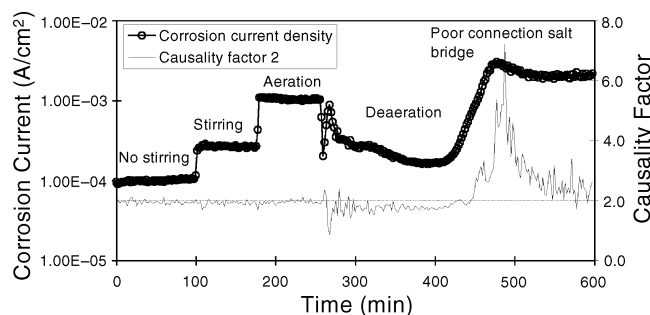


FIGURE 16. Corrosion rates for mild steel in 0.5 M NaCl under different hydrodynamic conditions.

REFERENCES

1. J. Dévay, L. Mészáros, *Acta Chim. Acad. Sci. Hung.* 100 (1979): p. 183.
2. L. Mészáros, G. Mészáros, B. Lengyel, *J. Electrochem. Soc.* 141 (1994): p. 2,068.
3. J.S. Gill, M. Callow, J.D. Scantlebury, *Corrosion* 39 (1983): p. 61.
4. S. Sathyanarayanan, K. Balakrishnan, *Brit. Corros. J.* 29 (1994): p. 152.
5. A. Pirnát, L. Mészáros, B. Lengyel, *Corros. Sci.* 37 (1995): p. 963.
6. M.C.H. McKubre, B.C. Syrett, ASTM STP908, “Harmonic Impedance Spectroscopy for the Determination of Corrosion Rates in Cathodically Protected Systems,” in *Corrosion Monitoring in Industrial Plants Using Nondestructive Testing and Electrochemical Methods*, eds. G.C. Moran, P. Labine (West Conshohocken, PA: ASTM, 1986), p. 433.
7. J.R. Macdonald, *Impedance Spectroscopy Emphasizing Solid Materials and Systems* (New York, NY: John Wiley and Sons, 1987), p. 267.

8. N.G. Thompson, K.M. Lawson, "Development of an Advanced Corrosion Rate Monitor," EPRI Report, TR-107867 (Palo Alto, CA: EPRI, 1997).
9. P. Wambacq, W. Sansen, *Distortion Analysis of Analog Integrated Circuits* (Boston, MA: Kluwer, 1998).
10. W. Sansen, K.U. Leuven, correspondence to author, August 1998.
11. G.P. Rao, A.K. Mishra, *J. Electroanal. Chem.* 77 (1977): p. 121.
12. U. Bertocci, *Corrosion* 35 (1979): p. 211.
13. L. Mészáros, J. Dévay, *Acta Chim. Acad. Sci. Hung.* 105 (1980): p. 1.
14. R.W. Bosch, W.F. Bogaerts, *Corrosion* 52, 3 (1996): p. 204.
15. R.W. Bosch, J. Hubrecht, W.F. Bogaerts, "Online Corrosion Monitoring Using Electrochemical Frequency Modulation (EFM)," EPRI Report, TR-112786 (Palo Alto, CA: EPRI, 1999).
16. Graphical Programming Software, LabVIEW, v. 3.01 (Austin, TX: National Instruments Corporation, 1994).
17. Graphical Programming Software, LabVIEW, Function and VI Reference Manual (Austin, TX: National Instruments Corporation, 1997).
18. M. Cerna, A.F. Harvey, "The Fundamentals of FFT-Based Signal Measurement," Proc. DSP[®] Exposition and Symp., held October 5-7 (Austin, TX: 1993), p. 171.
19. K. Fahy, E. Pérez, *Fast Fourier Transforms and Power Spectra in LabVIEW*, Application Note 040 (Austin, TX: National Instruments Corporation, 1993).
20. G. Trabanelli, V. Cassiti, "Mechanism and Phenomenology of Organic Inhibitors," in *Advances in Corrosion Science and Technology*, vol. 1, eds. M.G. Fontana, R.W. Staehle (New York, NY: Plenum Press, 1970), p. 147.
21. G. Trabanelli, *Corrosion* 47 (1991): p. 410.

CORROSION RESEARCH CALENDAR

CORROSION is a technical research journal devoted to furthering the knowledge of corrosion science and engineering. Within that context, *CORROSION* accepts notices of calls for papers and upcoming research grants, meetings, symposia, and conferences. All pertinent information, including the date, time, location, and sponsor of an event should be sent as far in advance as possible to: Angela Jarrell, Managing Editor, *CORROSION*, 1440 South Creek Drive, Houston, TX 77084-4906. Notices that are not accompanied by the contributor's name, daytime telephone number, and complete address will not be considered for publication.

2001

January 29-February 1 — 87th Annual Meeting of the Pulp and Paper Technical Association of Canada — Montreal, Quebec, Canada; Contact Glen D. Black, Phone: 514/392-6967; Fax: 514/392-0369; E-mail: gblack@paptac.ca.

* **February 12-14 — 9th Middle East Corrosion Conference — Bahrain;** Contact Bahrain Society of Engineers, E-mail: mohandis@batelco.com.bh.

February 18-20 — 2001 A Coatings Odyssey, 25th Biennial Western Coatings Society Symposium — Anaheim, CA; Contact Henry Kirsch, 562/942-1833.

February 21-25 — 2nd International Exhibition and Conference on Concrete — Mumbai, India; Contact Gajanan M. Sabnis, Phone: 202/806-6580; E-mail: gms@sabnis.com.

* **February 26-28 — NACE Northern Area Western Conference — Anchorage, AK;** Contact John Daley, 907/343-0268.

* **March 11-16 — CORROSION/2001 — Houston, TX;** Contact NACE, 281/228-6200.

April 16-20 — 4th Latin American Biodeterioration and Biodegradation Symposium—4 LABS — Buenos Aires, Argentina; Contact Blanca Rosales, Phone: +54 11 4709 3621; Fax: +54 11 47093210; E-mail: brosales@citefa.gov.ar.

* **May 1-3 — Western States Corrosion Seminar — Pomona, CA;** Contact Bill Stead, 909/982-8686.

* **May 8-9 — Symposium on Outdoor and Indoor Corrosion — Phoenix, AZ;** Contact Dorothy Fitzpatrick, 610/832-9677.

June 10-14 — 7th European Conference on Advanced Materials and Processes — Rimini, Italy; Contact Organizing Secretariat, Associazione Italiana di Metallurgia (AIM), Phone: +39 02 7602 1132; Fax: +39 02 7602 0551.

* **June 17-20 — 5th International Symposium on Superalloys 718, 625, 706 and Derivatives — Pittsburgh, PA;** Contact Marlene Karl, Phone: 724/776-9000, ext. 232; Fax: 724/776-3770; E-mail: karl@tms.org.

June 17-21 — American Water Works Association Annual Conference and Exposition — Washington, DC; Contact AWWA, 303/347-6160.

June 17-22 — 5th Electrochemical Impedance Spectroscopy Symposium — Marilleva, Trento, Italy; Contact Pier Luigi Bonora, Phone: +39 0461 882428; Fax: +39 0461 881966; E-mail: Pierluigi.Bonora@ing.unitn.it.

July 16-20 — 2001 U.S. Navy and Industry Corrosion Technology Information Exchange and Exhibits — Louisville, KY; Contact Don Hileman, Phone: 502/364-5231; Fax: 502/364-5354; E-mail: hilemande@nswcl.navy.mil.

* **August 5-9 — 10th International Conference on Environmental Degradation of Materials in Nuclear Power Systems—Water Reactors — Lake Tahoe, NV;** Contact NACE, 281/228-6200.

* **August 21-24 — 10th International Symposium on Corrosion in the Pulp and Paper Industry — Helsinki, Finland;** Contact Tero Hakkarainen, Phone: +358 9 456 5410; Fax: +358 9 456 7002; E-mail: tero.hakkarainen@vtt.fi.

* **August 26-29 — NACE Northern Area Eastern Conference — Halifax, NS, Canada;** Contact Don Marchand, Phone: 902/883-2220; Fax: 902/758-3622.

* **September 9-14 — NACE Fall Committee Week — Phoenix, AZ;** Contact NACE, 281/228-6200.

September 16-21 — International Conference on Hydrogen Effects on Material Behavior and Corrosion Deformation Interaction — Moran, WY; Contact Gary Was, Phone: 734/763-4675; Fax: 734/763-4540; E-mail: gsw@umich.edu.

* **September 18-20 — NACE UK Section Joint Conference with ICORR — Edinburgh, Scotland;** Contact Colin Britton, Phone: +44(0) 1635 202329; Fax: + 44 (0) 1635 202943; E-mail: Cbrit79727@aol.com.

* **September 23-28 — NACE Philadelphia Section, 2001 Liberty Bell Corrosion Course and Eastern Area Conference — Atlantic City, NJ;** Contact Emer C. Flounders, Jr., 215/658-0238; or Jack Wink, 856/461-6906.

* Sponsored or cosponsored by NACE International.